Journal of Materials Chemistry C

PAPER

View Article Online
View Journal

Cite this: DOI: 10.1039/c8tc02686f

Combining inverse and conventional pyroelectricity in antiferroelectric thin films for energy conversion†

Brendan Hanrahan, *[a] Yomery Espinal,[ab] Shi Liu,[a] Zeyu Zhang,[c] Alireza Khaligh,[c] Andrew Smith[d] and S. Pamir Alpay[b]

Pyroelectric materials are promising for thermal energy scavenging from waste-heat sources and new materials with exotic properties are constantly being discovered. Antiferroelectrics (AFE) are of particular interest since such materials have been observed to possess both conventional, negative pyroelectricity and inverse, positive pyroelectricity. In this study, we compare direct and indirect measurements of the pyroelectric coefficient and use the temperature dependence on the dielectric constant to show the inverse pyroelectric regime arises primarily from field-induced pyroelectricity. Energy conversion cycles are performed in both pyroelectric regimes using a 1 kHz pulsed laser heat source, realizing a maximum power density of 2.25 W cm^{-3} in the conventional regime and 0.68 W cm^{-3} in the inverse regime. A new pyroelectric energy conversion model, using parameters taken from direct measurements of the pyroelectric coefficient, capacitance, loss tangent, and leakage current agrees with the energy conversion experiments, showing both the validity of the model and the origin of pyroelectricity in the inverse regime. Finally, a resonant circuit for pyroelectric energy harvesting is proposed that takes full advantage of the bi-directional functionality of AFE materials. This work clarifies the debate on the origin of pyroelectric features in AFE materials and demonstrates the potential for future energy conversion applications.

Received 1st June 2018,
Accepted 28th August 2018

DOI: 10.1039/c8tc02686f

rsc.li/materials-c

Introduction

The electrothermal coupling of ferroelectrics (FE) and antiferroelectrics (AFE) make them attractive for energy harvesting and solid-state cooling applications. Thin film versions of these materials are of particular interest owing to their ability to withstand high electric fields, increasing the potential for work in an energy conversion cycle. One of the first thin films identified to possess a significant energy conversion potential is AFE lead zirconate titanate. This material was calculated to have an electrocaloric adiabatic cooling potential of 12 K at 420 kV cm^{-1} applied electric fields.[1] More recently, Geng *et al.* explored the electric-field driven AFE/FE phase transition in $(Pb_{0.97}La_{0.02})(Zr_{0.95}Ti_{0.05})O_3$ and found giant inverse pyroelectricity, suggesting the spontaneous polarization increases with an increasing temperature.[2]

AFE materials have been of interest since 1950s when their characteristic double hysteresis loop was first observed in $PbZrO_3$.[3] Kittel proposed the mechanism for AFE materials containing an anti-polar ground state and an electric field-driven AFE/FE phase transition where the anti-polar arrangement has a center of symmetry, effectively cancelling the primary piezoelectric and pyroelectric effects.[4] Pyroelectricity in AFE materials was first explored by Ujma *et al.* in the vicinity of the AFE/FE phase transition.[5] Yang *et al.* showed that the FE transition point could be manipulated under certain electric fields and temperatures observed with pyroelectric current measurements.[6] Using indirect measurements, Hao showed pyroelectric coefficients reaching 8400 μC m^{-2} K^{-1} at the AFE/FE transition.[7]

Inverse caloric effects, where temperature decreases under an applied field, are directly related to the inverse pyroelectric effect and are of significant interest from both a fundamental and applications perspective. In elastocalorics this behavior has been observed in the vicinity of the martensitic transition, enhanced by the addition of Cu doping.[8] Interestingly, giant inverse magnetocaloric effects, on the order of the primary

[a] Sensors & Electron Devices Directorate, U.S. Army Research Laboratory, Adelphi, MD 20783, USA. E-mail: brendan.m.hanrahan.civ@mail.mil
[b] Department of Material Science & Engineering, Institute of Materials Science, University of Connecticut, Storrs, CT, 06269, USA
[c] Department of Electrical and Computer Engineering, University of Maryland, College Park, MD, 20742, USA
[d] Mechanical Engineering Department, US Naval Academy, Annapolis, MD, 21402, USA

† Electronic supplementary information (ESI) available. See DOI: 10.1039/c8tc02686f

coefficient magnitude, have also been observed at a martensitic transition phase transition.[9] Barium titanate displays both inverse electrocaloric[10] and barocaloric[11] behavior at temperatures approaching a structural phase transition. Inverse or negative electrocalorics have been directly measured on relaxor ferroelectrics[12] and in other ferroelectrics, generally where an increase in temperature transitions the materials from a lower to higher polarization state.[13]

In this work we directly measure the pyroelectric coefficient of $(Pb_{0.995}La_{0.005})(Zr_{0.95}Ti_{0.05}O_3)$ (denoted as PLZT) across the electric field-driven AFE/FE transition and find that its magnitude and relationship with electric field vary significantly when compared to expectations from indirect measurements of adiabatic polarization–electric field hysteresis loops. Separate measurements of auxiliary pyroelectric effects elucidate the origin of inverse pyroelectricity in AFE PLZT arising primarily from the field-induced pyroelectricity. We then model and perform energy conversion cycles in the inverse and conventional regimes of the pyroelectricity, demonstrating the possibility for multi-cycle conversion within a single material system. We start by comparing the direct and indirect measurements of pyroelectric coefficients in AFE PLZT. It is known that indirect measurements of pyroelectricity from isothermal hysteresis loops are unable to capture electric field, strain-dependent, or extrinsic contributions to pyroelectric coefficient, which direct measurements capture.[14,15] Direct measurements of pyroelectricity are obtained by combining the electric field dependence of peak pyroelectric current under pulsed laser heating with measurements of pyroelectric current under periodic heating (details provided in the Experimental section).

Results and discussion

Fig. 1a shows a characteristic AFE polarization–electric field hysteresis loop and the pyroelectric coefficient hysteresis obtained from the direct measurement. As shown in Fig. 1a, starting at zero field, the material has increasing polarization and positive pyroelectric coefficient with increasing electric fields. The pyroelectric coefficient starts decreasing when the electric field becomes larger than 235 kV cm^{-1} whereas the polarization keeps increasing. This suggests the coexistence of FE and AFE phases where the inverse pyroelectricity associated with AFE phase is partly cancelled by the conventional pyroelectricity associated with the FE phase.[16] The pyroelectric coefficient eventually becomes negative with increasing magnitude at higher electric field. From here, the pyroelectric coefficient hysteresis is dominated by the fraction of switched domains, similar to observations in other PZT thin films.[14] The latency in the electric field-driven phase transition can also be observed as the electric field returns to zero where the AFE/FE transition happens at a lower field. Interestingly, the peak pyroelectric coefficient is asymmetrical with electric field, whereas the dielectric hysteresis measurements are always symmetrical, which could indicate this sample has a preferential polarization direction.[14,17]

The pyroelectric coefficient differs drastically in both magnitude and electric field dependence between the direct and indirect measurement techniques (Fig. 1b). The source of this difference is rooted in the fact that the indirect technique measures the polarization dependence with electric field at a specific background temperature, while the direct measurement is using temperature perturbations and measuring current at static applied fields. The indirect method is particularly susceptible to artifacts in AFE materials, where there is a temperature-dependent, electric-field driven AFE/FE transition which is measured during the polarization hysteresis. Time-dependence is not expected to be the source of difference between the two techniques, where the indirect measurement is at thermal equilibrium and the direct measurements use thermal signals ranging from 10 °C s^{-1} (hotplate) to ~1000 °C s^{-1} (laser) heating rates but this merits further study.

The origin of inverse pyroelectricity and the intimately related inverse electrocaloric effect remain controversial. For polar materials,

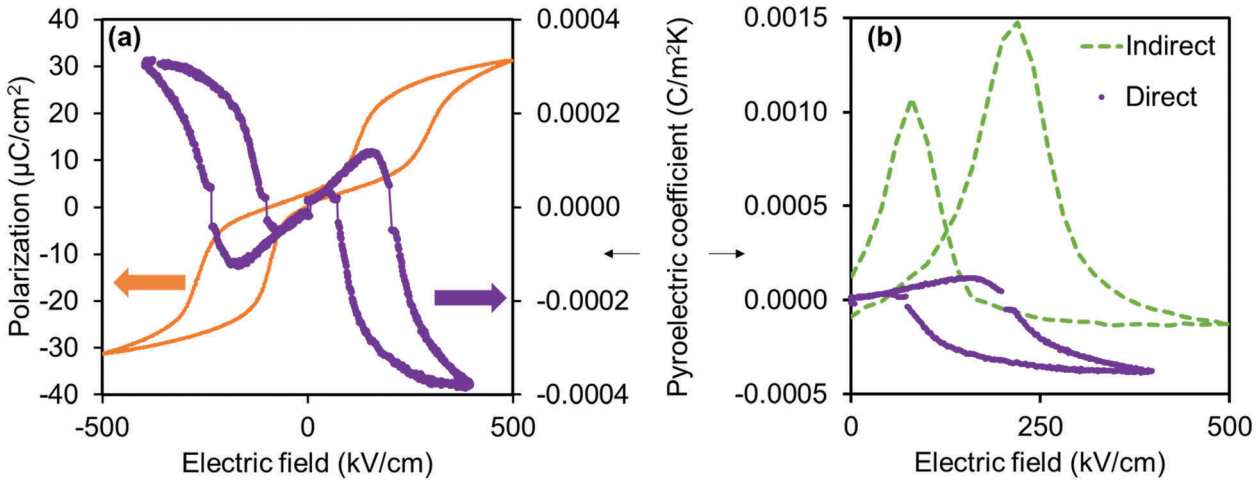

Fig. 1 (a) The polarization and pyroelectric coefficient hysteresis measurement for thin film AFE PLZT at room temperature. (b) Comparison of the pyroelectric coefficients obtained from direct measurement (solid line) with predictions from isothermal hysteresis loops (dashed line).

the dominant effect stems from the change of the spontaneous polarization in response to the change in temperature, referred to as the intrinsic pyroelectricity. Dielectric materials under an applied electric field can also give rise to the pyroelectric effect because of the temperature (T) dependent dielectric constant (ε), as described by eqn (1), referred to as field-induced pyroelectricity (Π_{FI}).

$$\Pi_{FI} = \varepsilon_0 E\left(\frac{\partial \varepsilon}{\partial T}\right)_x \quad (1)$$

where the electric field (E) is applied at constant strain (x) and ε_0 is the permittivity of free space. Inverse pyroelectricity in AFE materials has been considered an intrinsic effect and is attributed to an asymmetry in rotation between anti-polar vectors upon heating, leading to a net-repolarization of the material under an external electric field.[2] However, the temperature dependence on the dielectric constant can also lead to a net observed inverse pyroelectric effect in the presence of an applied field. This property gives rise to "dielectric bolometers"[18] and typically has a positive sign in FEs leading up to the Curie temperature and a negative sign following in the paraelectric (PE) phase. It is not clear in AFEs which term, primary or field-induced, is responsible for the observed inverse pyroelectric response.

In order calculate the pyroelectric coefficient, a phenomenological theory of phase transformations is used to understand and describe the temperature dependence of dielectric susceptibility and its connection to the field-induced pyroelectricity. For an AFE material, the Landau–Kittel free energy functional (f) can be represented by a two sublattice model:[19]

$$f = \frac{1}{2}a\left(D_1^2 + D_2^2\right) + \frac{1}{4}b\left(D_1^4 + D_2^4\right) + \frac{1}{6}c\left(D_1^6 + D_2^6\right) + gD_1D_2 - (D_1 + D_2)E. \quad (2)$$

where D_1 and D_2 are the dielectric displacement components at sublattices 1 and 2, respectively; a, b, c, and g are the dielectric stiffness (or Landau) coefficients. The total dielectric displacement (D) is given by $D_1 + D_2$ and the electric field component is parallel to the total dielectric displacement. In this phenomenological model, the dimensionless, Landau-type expansion coefficients are defined as follows: $a = g + a_1(T - T_0)$, $a_1 = 1$, $b = c = 1/3$, where $g = 0.5$ characterizes the AFE coupling strength and $T_0 = 1$ is the paraelectric-to-antiferroelectric transition temperature in zero field.[19] These parameters are not specific to any antiferroelectric and their values are chosen to give a qualitative prediction of the AFE/PE phase transition under zero field and the field-induced AFE/FE/PE phase transition as demonstrated in ref. 19.

For given values of electric field and temperatures, the thermodynamic equilibrium values of D_1 and D_2 are determined by finding the lowest free energy with the grid search method in the parameter space of $D_1 \geq 0$ and $-D_1 \leq D_2 \leq D_1$. It is straightforward to derive from the equation of free energy that the dielectric susceptibility (χ) is given by:

$$\chi = \left(\frac{\partial D}{\partial E}\right)_T = \frac{d_1 + d_2 - 2g}{d_1 d_2 - g^2} \quad (3)$$

and the total pyroelectric coefficient (Π_{total}) is:

$$\Pi_{total} = \left(\frac{\partial D}{\partial T}\right)_E = \Pi_1 + \Pi_2 = \frac{a_1 g(D_1 + D_2) - a_1(D_1 d_2 + D_2 d_1)}{d_1 d_2 - g^2} \quad (4)$$

where $d_i = a + 3bD_i^2 + 5cD_i^4$ for $i = 1, 2$. The temperature derivative of dielectric susceptibility is then:

$$\frac{\partial \chi}{\partial T} = \frac{(d_{11} + d_{22})(d_1 d_2 - g^2) - (d_1 + d_2 - 2g)(d_{11} d_2 + d_1 d_{22})}{(d_1 d_2 - g^2)^2} \quad (5)$$

where $d_{ii} = a_1 + 6bD_i\Pi_i + 20cD_i^3\Pi_i$ for $i = 1, 2$.

Values of Π_{total} and Π_{FI} were compared to understand the effect of temperature-dependent dielectric response on the pyroelectricity (Fig. 2a). At low electric fields these two quantities are nearly identical, suggesting the field-induced pyroelectric coefficient is the dominant effect responsible for inverse pyroelectricity. In this field region, the AFE system can largely

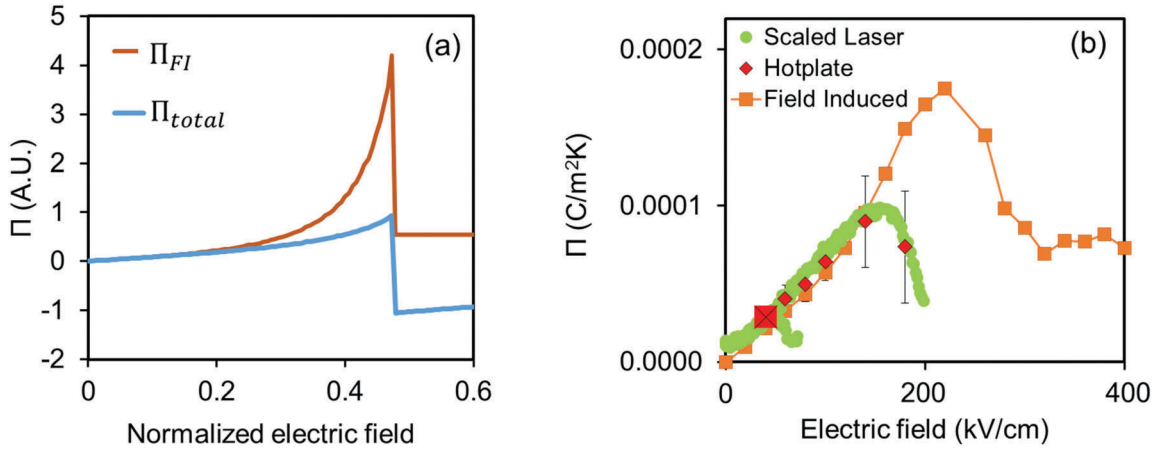

Fig. 2 (a) A comparison of the calculated field-induced and total pyroelectric coefficients from phenomenological theory. (b) Pyroelectric coefficient at positive biases comparing directly measured values (diamonds) and the scaled coefficient (circles) with the field-induced pyroelectricity calculated from eqn (1) using the direct temperature derivative permittivity.

be considered as a linear dielectric wherein the total macroscopic polarization is dominated by the field-induced polarization. With increasing electric fields, the values of Π_{total} and Π_{FI} start to diverge. This suggests the emergence of the FE response and thus the conventional pyroelectricity with a negative coefficient before reaching the critical electric field.

Fig. 2b shows the experimentally-isolated field-induced pyroelectric coefficient, calculated from directly measured temperature dependent dielectric constant values in eqn (1), along with the pyroelectric coefficient obtained from the scaled pulsed laser test, which are the sum of all active pyroelectric effects, as well as the hotplate tests measurements used for scaling. Consistent with the model prediction based on the phenomenological Landau theory, there is very good agreement between the field-induced pyroelectric coefficient and the directly measured coefficients at low fields. This confirms that the field-induced pyroelectricity is responsible for the inverse pyroelectricity in PLZT. It is noted that this also explains the scaling law for electrocaloric temperature changes in AFE systems where the temperature change is quadratic in the electric field.[20] As the material begins to transition from the AFE phase to a non-centrosymmetric FE at higher fields, the negative intrinsic coefficient gets added to the field-induced coefficient, reducing the magnitude of the total pyroelectric response as observed by the divergence between the direct pyroelectric measurement and calculated field-induced coefficient in both the theory and measurements. At increasing fields, there is a cross-over where the intrinsic coefficient of the FE phase equals and then exceeds the inverse coefficient at $\sim$200 kV cm^{-1}. The location of this cross-over does not map precisely with the AFE/FE transition electric field which was measured at 300 kV cm^{-1} (Fig. 1a) indicating the presence of FE phase before it is observed in the dielectric hysteresis.

The conventional and inverse coefficients can both be harnessed for pyroelectric energy conversion (PEC). The energy conversion process is most efficient when synchronous application of thermal and electric field waveforms closely resembles a thermodynamic cycle. In general, this cycle consists of four processes: charging, heating, discharging, and cooling. The specific path of these processes, for example isothermal *vs.* adiabatic charging, will give differences in cycle efficiency and power density.[21] Operating pyroelectrics in this manner was first proposed by Margosian for a space-based application using a Stirling cycle[22] and then refined by Olsen[23–25] who provided a comprehensive comparison of different cycles with real-world benefits and challenges. Sebald *et al.* provided the most thorough translation of the pyroelectric material coefficients into their thermodynamic counterparts.[26] The power density (P_{cycle}) of any pyroelectric cycle can be calculated analytically as,

$$P_{cycle} = \Pi_{total}(E)\cdot\Delta T\cdot\Delta E\cdot f \quad (6)$$

where $\Pi_{total}(E)$ is the total pyroelectric coefficient with the electric field dependence, and f is frequency.[27] The electrical losses during the cycle can be divided into AC and DC components, where the AC power losses during the charging and discharging processes are,[28]

$$P_{C-D} = \frac{C(E)\cdot\Delta E^2\cdot\tan\delta(E)\cdot f\cdot A\cdot d}{\pi} \quad (7)$$

where $C(E)$ and $\tan\delta(E)$ are the electric field dependent capacitance and loss tangent of the material, respectively. A is the device area and d is the thickness. The power density of the DC losses is due to leakage current and can be described as,

$$P_{leak} = E_{avg}\cdot J(E) \quad (8)$$

where E_{avg} is the average cycle electric field and $J(E)$ is the electric field-dependent leakage current density. From here, an energy balance can be performed where,

$$P_{total} = P_{cycle} + P_{C-D} + P_{leak} \quad (9)$$

One interesting feature to note is how the electric field dependence of material coefficients dictate the total power density at a given applied field. AFE materials provide a particularly rich experimental space to explore the energy balance due to the electric field-induced AFE/FE phase transition. Also, to date, the inverse pyroelectric coefficient realized in AFE materials has not been used for PEC, while there have been some examples of inverse pyroelectricity used in electrocaloric devices.[19] Accurate measurement of the pyroelectric coefficient and its relationship with electric field is critical to understanding the fundamental mechanisms of observed pyroelectric properties and harnessing them for electrothermal energy conversion.

For the first time, we use the inverse region in a PEC device. PEC cycles are run using a pulsed 1.5 μm IR laser synchronized with an electric field waveform at 1 kHz, shown in Fig. 3a, using the technique described in ref. 29. The electric field is operated as a near-triangle wave to minimize the current during charging and discharging the capacitor while allowing for heating and cooling to take place nearly isoelectricly in the flattened peaks of the waveform. The laser heated sample, which is in intimate contact with the substrate, has a thermal relaxation time of $\sim$6 μs measured from the pyroelectric current during free cooling of the system. The implications of the inverse pyroelectric coefficient for energy conversion are that the cycle needs to be phase shifted 180° from the normal cycle (Fig. 3a), *i.e.*, charge → cool → discharge → heat. The magnitude and direction of the pyroelectric current during the heating/cooling processes is in agreement with what is predicted by the measurements of $\Pi(E)$ (Fig. 1a).

The average voltage was varied from 0.5 to 19.5 V in 1 V intervals while the peak-to-peak voltage was held at 1 V to minimize the variance in materials properties within a given PEC cycle. At the point of the pyroelectric coefficient crossover, the phase of the cycle was shifted. The variation of power density with applied electric field is shown in Fig. 3b. Each power density is the average of 200 cycles. Eqn (9) was used to model the energy conversion potential using the measured electric field-dependent pyroelectric coefficient, capacitance, and loss tangent (Fig. 1a and Fig. S5, ESI†). The model is in good agreement with the measured power conversion density for voltages less than 15 V (300 kV cm^{-1}). Above 15 V, it was found that leakage current loss manifested inconsistently during the energy conversion tests, sometimes increasing to a level that resulted in net power loss. At very low fields, the pyroelectric coefficient is minimized and the loss tangent is high and variable, which is why we see

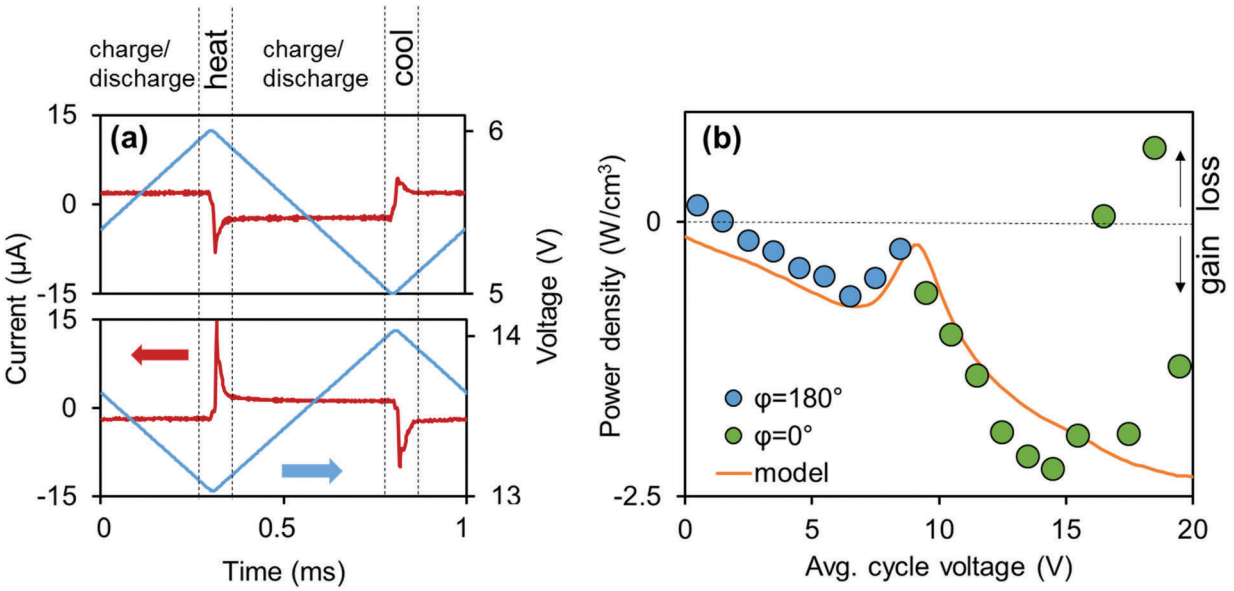

Fig. 3 (a) PEC cycles measured in the inverse (5–6 V) and conventional (13–14 V) regimes annotated with the energy conversion cycle. (b) Measured power density of PEC over a range of average voltage compared with model using measured material properties. Above 15 V leakage current unpredictably affected performance.

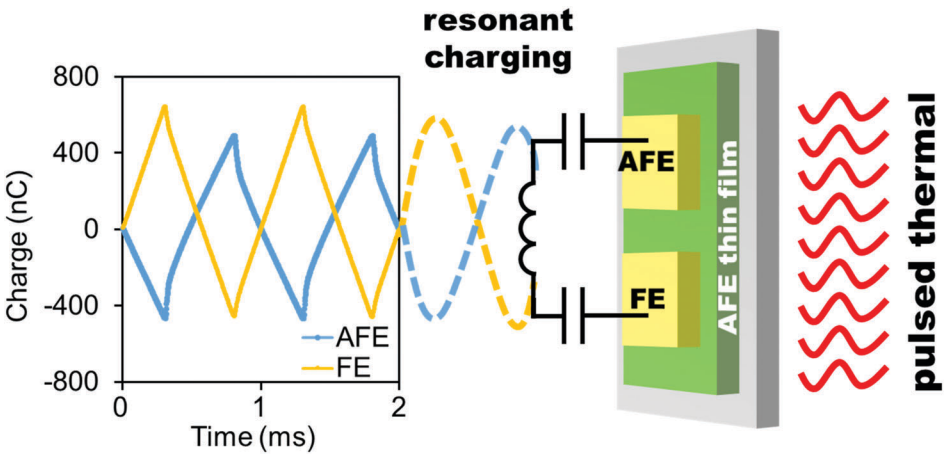

Fig. 4 (left) Charge measured from two laser-driven PEC cycles in the AFE and FE regimes on PLZT film. (right) Extending the charge curves highlights a PEC device with the potential for resonant charging between AFE and FE regimes on a single thin film by synchronizing heating/cooling processes.

some disagreement between the model and experiments. The peak power density in the inverse regime is 30% of the peak in the primary regime, despite having only 25% of the magnitude of a pyroelectric coefficient. This difference arises from the charge–discharge losses at each point in the cycle, which illustrates the need to consider more than the pyroelectric coefficient for PEC applications. The bi-directional pyroelectric coefficient enables energy converter designs not possible with normal pyroelectrics. If both FE and AFE regimes are realized on a single device, the 180° phase shift of the conversion cycle for the inverse AFE regime means the charging and discharging of each device happens simultaneously (Fig. 3a and 4), enabling circuit topologies where charge can be shared. A single material could be biased to a voltage that optimizes power density for the AFE or FE regime by adding a second set of passive capacitors to each AFE or FE device. As a LC resonant circuit, the two devices would charge each other efficiently when the switch is closed and undergo thermal excitation simultaneously, as described in Fig. 4.

Conclusions

If considering pyroelectrics as a heat engine analog where electric field is thermodynamically equivalent to pressure, the resonant charge sharing between capacitors would be like offsetting the pistons in a car engine, where the expansion of one cylinder drives the compression of the opposite cylinder. This elegant circuit, taking advantage of the thermodynamic relation of the two devices, could have increased power density

compared to a resonant circuit with only one active pyroelectric capacitor. The proposed circuit can achieve much higher efficiency than the reported full-bridge rectifier pyroelectric system[30,31] because the pyroelectric material undergoes electric field cycling in addition to temperature variation, dramatically increasing the energy density of conversion.[21] The replacement of a passive storage capacitor with an active AFE capacitor scales the power density, in this case it would increase 30% by adding our maximum measured inverse regime power density (0.68 W cm^{-3}) to our maximum measured conventional regime (2.25 W cm^{-3}). Further work is needed towards realizing practical PEC.

The dual sign convention of the pyroelectric response of AFE thin films is analyzed from both a fundamental and application perspective. Direct measurement of the pyroelectric coefficient disagrees with expectations from indirect measurements, *i.e.*, pyroelectric coefficients derived from isothermal hysteresis tests. In the inverse regime, the indirect measurement dramatically overestimates the measured coefficient. The origin of the inverse regime is found to be the temperature dependence on the dielectric constant, which can lead to a field-induced pyroelectric effect. The electrothermal energy conversion potential of AFE thin films have been explored in both the conventional and inverse regimes of the pyroelectric coefficient. Measurements of the electric field-dependent pyroelectric coefficient, capacitance, loss tangent, and leakage current are used to predict the energy conversion power density for laser-driven PEC cycles. Experimental conversion cycles agree well with the model, realizing a maximum power density of 2.25 W cm^{-3} in the primary regime and 0.68 W cm^{-3} in the inverse regime running phase-shifted cycles. This work clarifies the potential for useful application of the inverse pyroelectric regime as well as validates a property-dependent pyroelectric conversion model.

Experimental details

Material growth and deposition

La-Doped PZT with a Zr : Ti ratio of 95 : 5 is used for this study. A small amount of Lanthanum (0.5 at%) is added to the solution to reduce the leakage current.[32] The 500 nm thick PLZT film is chemical solution-deposited on a platinized silicon wafer. Further process details are found in the ESI.† PLZT films are coated with a nanostructured IrO_2 thin film, serving the dual purpose of top electrode and infrared absorber for the laser-heated energy conversion cycles. Temperature dependent X-ray diffraction shows the films are crystalline (Fig. S1, ESI†). The IrO_2 films are grown in a reactive DC sputtering process to a thickness of $\sim$700 nm. A cross section SEM of the device is provided in Fig. S2, ESI.† On-chip thin film Pt traces are used as resistive thermal devices (RTDs) for temperature measurements during material characterization tests.

Materials characterization

For the indirect measurement of pyroelectricity, the polarization relationship with temperature is calculated at various applied fields from isothermal hysteresis loops taken from 27 to 200 °C (Fig. S3, ESI†). Direct pyroelectric measurement of the pyroelectric coefficient is accomplished through a two-step process. First, the sample is heated with a 50% duty cycle, square laser pulse with 1 μS rise time at a frequency of 1 kHz while simultaneously being stimulated by a $\pm$20 V triangle wave electrical bias at 1 Hz. The pyroelectric and polarization current are simultaneously measured at 10^6 samples per s by a data acquisition system. The polarization current, which is on the order of 100 nA, is removed from the measured current, leaving only the pyroelectric current, on the order of 1–4 μA. This test gives the electric field dependence on the peak pyroelectric current under laser heating.

To obtain the pyroelectric coefficient, the temperature of the sample is oscillated at 1 Hz *via* cartridge heater beneath the sample while temperature is measured on the surface of the chip with the RTD and sample current is monitored, using the equation from Byer and Roundy:[33]

$$\Pi = I \cdot \frac{dt}{A \cdot dT} \tag{10}$$

Characteristic data is shown in Fig. S4, ESI.† This process is repeated at increasing, static electric fields, allowing the sample to return to zero applied field between each measurement. With increasing electric fields, auxiliary, non-pyroelectric currents increase, therefore this process is limited to $<$10 V (200 kV cm^{-1}). A least-squares fit is then used to scale the peak pyroelectric current from the laser test, which is much less sensitive to non-pyroelectric currents, to the pyroelectric coefficient measurements from the hotplate.

The small signal capacitance and loss tangent were measured at 10 kHz and $\pm$20 V in 0.2 V increments (Fig. S5a and b, ESI†). The leakage current was calculated from the average measured current during a 100 ms time period after a 4 s soak at a given voltage, in a manner described in ref. 34 (Fig. S5c, ESI†). The loss tangent follows similar behavior with an average value of 2%, similar to what has been reported in literature.[1] Leakage current varies by four orders of magnitude over the range of tested voltages. To measure the temperature differential dielectric constant, the dielectric constant of the sample is monitored with a 10 kHz, 5 mV sinusoidal probe signal while the sample is heated. The temperature from room temperature to $\sim$60 °C, monitored with the on-chip RTD, and dielectric constant are measured simultaneously. This process is repeated over a range of DC electric fields.

Conflicts of interest

There are no conflicts to declare.

Acknowledgements

The authors would like to thank Mr C. Neville for his helpful discussions regarding the PEC model and Dr M. Graziano for discussions regarding the XRD analysis.

Notes and references

1 A. S. Mischenko, Q. Zhang, J. F. Scott, R. W. Whatmore and N. D. Mathur, *Science*, 2006, **311**, 1270–1271.
2 W. Geng, Y. Liu, X. Meng, L. Bellaiche, J. F. Scott, B. Dkhil and A. Jiang, *Adv. Mater.*, 2015, **27**, 3165–3169.
3 E. Sawaguchi, H. Maniwa and S. Hoshino, *Phys. Rev.*, 1951, **83**, 1078.
4 C. Kittel, *Phys. Rev.*, 1951, **82**, 729–732.
5 Z. Ujma and J. Handerek, *Ferroelectrics*, 1981, **33**, 37–42.
6 Y. Tongqing, L. Peng, X. Zhuo, Z. Liangying and Y. Xi, *Ferroelectrics*, 1999, **230**, 181–186.
7 X. Hao, J. Zhai, L. B. Kong and Z. Xu, *Prog. Mater. Sci.*, 2014, **63**, 1–57.
8 A. Wójcik, W. Maziarz, M. J. Szczerba, M. Sikora, A. Żywczak, C. O. Aguilar-Ortiz, P. Álvarez-Alonso, E. Villa, H. Flores-Zúñiga, E. Cesari, J. Dutkiewicz and V. A. Chernenko, *J. Alloys Compd.*, 2017, **721**, 172–181.
9 T. Krenke, E. Duman, M. Acet, E. F. Wassermann, X. Moya, L. Mañosa and A. Planes, *Nat. Mater.*, 2005, **4**, 450.
10 M. Marathe, D. Renggli, M. Sanlialp, M. O. Karabasov, V. V. Shvartsman, D. C. Lupascu, A. Grünebohm and C. Ederer, *Phys. Rev. B*, 2017, **96**, 014102.
11 E. Stern-Taulats, P. Lloveras, M. Barrio, E. Defay, M. Egilmez, A. Planes, J.-L. Tamarit, L. Mañosa, N. D. Mathur and X. Moya, *APL Mater.*, 2016, **4**, 091102.
12 J. Peräntie, J. Hagberg, A. Uusimäki and H. Jantunen, *Phys. Rev. B: Condens. Matter Mater. Phys.*, 2010, **82**, 134119.
13 B. Peng, H. Fan and Q. Zhang, *Adv. Funct. Mater.*, 2013, **23**, 2987–2992.
14 B. Hanrahan, Y. Espinal, C. Neville, R. Rudy, M. Rivas, A. Smith, M. T. Kesim and S. P. Alpay, *J. Appl. Phys.*, 2018, **123**, 124104.
15 S. Jachalke, E. Mehner, H. Stöcker, J. Hanzig, M. Sonntag, T. Weigel, T. Leisegang and D. C. Meyer, *Appl. Phys. Rev.*, 2017, **4**, 021303.
16 N. Novak, F. Weyland, S. Patel, H. Guo, X. Tan, J. Rödel and J. Koruza, *Physical Review B*, 2018, **97**, 094113.
17 A. G. Chynoweth, *J. Appl. Phys.*, 1956, **27**, 78–84.
18 R. A. Hanel, *The Dielectric Bolometer, A New Type of Thermal Radiation Detector*, Report NASA TN D-500, NASA Goddard Space Flight Center, 1960.
19 R. Pirc, B. Rožič, J. Koruza, B. Malič and Z. Kutnjak, *EPL*, 2014, **107**, 17002.
20 S. Lisenkov, B. K. Mani, E. Glazkova, C. W. Miller and I. Ponomareva, *Sci. Rep.*, 2016, **6**, 19590.
21 B. M. Hanrahan, F. Sze, A. N. Smith and N. R. Jankowski, *Int. J. Energy Res.*, 2017, **41**, 1880–1890.
22 P. M. Margosian, *Thermal electrostatic generator variable capacitance device for converting thermal energy to electric energy*, Report NASA-TN-D-2763, NASA, 1965.
23 R. B. Olsen, J. M. Briscoe, D. A. Bruno and W. F. Butler, *Ferroelectrics*, 1981, **38**, 975–978.
24 R. B. Olsen, D. A. Bruno and J. M. Briscoe, *J. Appl. Phys.*, 1985, **58**, 4709.
25 R. B. Olsen, D. A. Bruno, J. M. Briscoe and E. W. Jacobs, *J. Appl. Phys.*, 1985, **57**, 5036–5042.
26 G. Sebald, S. Pruvost and D. Guyomar, *Smart Mater. Struct.*, 2008, **17**, 015012.
27 R. Kandilian, A. Navid and L. Pilon, *Smart Mater. Struct.*, 2011, **20**, 055020.
28 A. N. Smith, B. M. Hanrahan, C. J. Neville and N. R. Jankowski, *J. Phys.: Conf. Ser.*, 2016, **773**, 012102.
29 B. Hanrahan, C. Neville, A. Smith, N. Ter-Gabrielyan, N. Jankowski and C. M. Waits, *Adv. Mater. Technol.*, 2016, 1600178, DOI: 10.1002/admt.201600178.
30 A. Sultana, M. M. Alam, T. R. Middya and D. Mandal, *Appl. Energy*, 2018, **221**, 299–307.
31 H. Zhang, Y. Xie, X. Li, Z. Huang, S. Zhang, Y. Su, B. Wu, L. He, W. Yang and Y. Lin, *Energy*, 2016, **101**, 202–210.
32 C. Sudhama, J. Kim, J. Lee, V. Chikarmane, W. Shepherd and E. R. Myers, *J. Vac. Sci. Technol., B: Microelectron. Nanometer Struct.–Process., Meas., Phenom.*, 1993, **11**, 1302–1309.
33 R. L. Byer and C. B. Roundy, *Ferroelectrics*, 1972, **3**, 333–338.
34 B. Hanrahan, L. Sanchez, C. M. Waits and R. G. Polcawich, *Smart Mater. Struct.*, 2016, **25**, 015025.